Acta Crystallographica Section B
Structural Science
ISSN 0108-7681

Structures of mono-unsaturated triacylglycerols. III. The β-2 polymorphs of *trans*-mono-unsaturated triacylglycerols and related fully saturated triacylglycerols

Jan B. van Mechelen,* Rene Peschar and Henk Schenk

University of Amsterdam, HIMS/FNWI/Kristallographie, Valckenierstraat 65, 1018 XE Amsterdam, The Netherlands

Correspondence e-mail: janvm@science.uva.nl

Received 10 January 2008
Accepted 19 February 2008

The β-2 crystal structures of a series of saturated and *trans*-mono-unsaturated triacylglycerols (TAGs) have been solved from high-resolution powder synchrotron diffraction data. The series comprises symmetric as well as asymmetric even-numbered TAGs and the *trans*-mono-unsaturated ones all have a single elaidoyl chain. The structures have been solved with the direct-space parallel-tempering program *FOX* and refined with the Rietveld program *GSAS*. The β-2 structures all crystallized in the space group $P\bar{1}$ with the same molecular conformation. Within the resolution of the data no significant difference in packing or conformation is observed between *trans*-mono-unsaturated TAGs and saturated (stearoyl or palmitoyl) chain-containing analogues, in spite of the lower melting points of the former. An analysis of the position of the stepped methyl end-plane in the various subgroups of TAGs confirms most but not all suppositions found in the literature.

1. Introduction

Natural fats and oils are mixtures of a large variety of triacylglycerols (TAGs), esterifications of glycerol with long-chain fatty acids. These fats and oils as well as the TAGs exhibit a complex temperature-dependent polymorphism, characterized by a set of crystallization and melting trajectories that are related to the principal types of acyl-chain packing modes, commonly denoted as the α, β' and β polymorph(s).

For application in food products such as margarines, shortenings *etc.*, natural oils are usually too highly unsaturated and too liable to oxidation. Nowadays, several industrial processes exist that can reduce the degree of unsaturation, and thus enhance the melting point, consistency and resistance to oxidation. One of these processes is hydrogenation, a technique that unfortunately also leads to isomerization of the mono-unsaturated *cis*-oleic acid (*cis*-9-octadecenoic acid; O) into its *trans* isomer elaidic acid (*trans*-9-octadecenoic acid; E; C18:1). The presence of the elaidoyl chain, one of the major *trans* fatty-acid chains, is suspected of increasing potential health risks because it resembles the stearoyl chain (S; C18:0). For example, when incorporated in membrane lipids elaidoyl chains can replace saturated chains and change the physicochemical properties of biological membranes (Björkbom *et al.*, 2007).

The β-2 form is the most stable polymorph of many saturated TAGs, amongst others the monoacid (n n n) class of TAGs and the classes (n n $n+2$) and (n $n+2$ $n+2$) (Hagemann, 1988). The monoacid (n n n) class of TAGs has been studied in most detail, using single-crystal data (n = 10, Jensen & Mabis, 1966; n = 12, Larsson, 1965; Gibon *et al.*, 1984; n = 16, van Langevelde *et al.*, 1999) as well as high-resolution synchrotron powder diffraction (HR-SPD) data (n = 14, 18;

van Langevelde *et al.*, 2001*a*; n = 13, van Langevelde *et al.*, 2001*b*; n = 15, 17, 19; Helmholdt *et al.*, 2002) and confirmed earlier postulations of the packing of this type of polymorph (Lutton, 1971, 1972; de Jong & van Soest, 1978). The single-crystal packing of the (n n n) analogue EEE[1] (Culot *et al.*, 2000) is also in accordance with this result.

Although packing models of saturated mixed-acid TAGs have been proposed (Lutton, 1971, 1972; de Jong & van Soest, 1978) and a structural study of the E-chain containing TAGs has been carried out (Elisabettini *et al.*, 1998), the precise influence of replacement of the saturated S-chain by an E-chain on their physical properties and packing are still not known.

Using HR-SPD data and the direct-space search program *FOX*, we obtained β-2 crystal structure models of a set of TAGs from the above-mentioned classes and their E-containing analogues. From the class (n n n) 1,3-distearoyl-2-elaidoylglycerol (SES) and 1,2-distearoyl-3-elaidoylglycerol (SSE), from the class (n n $n+2$) 1,2-dipalmitoyl-3-stearoylglycerol (PPS), 1,2-dipalmitoyl-3-elaidoylglycerol (PPE), 1,2-dimyristoyl-3-palmitoylglycerol (MMP) and 1,2-dilauroyl-3-myristoylglycerol (LLM), and from the class (n $n+2$ $n+2$) 1-palmitoyl-2,3-distearoylglycerol (PSS) and 1-lauroyl-2,3-dimyristoylglycerol (LMM). Also, β-2 crystal-structure models have been obtained for the β'-stable 1,3-dipalmitoyl-2-elaidoylglycerol (PEP) and 1,3-dipalmitoyl-2-stearoylglycerol (PSP).

The methyl end-planes in the various subgroups of TAGs were analyzed in relation to the observed melting points T_m. In the next paper of this series (paper IV, van Mechelen *et al.*, 2008), the β-2 crystal structure models will be compared with crystal structure models of the β' polymorphs of these and similar types of TAGs.[1]

2. Experimental

2.1. Samples, sample preparation and data collection

Samples of PEP, PPE, SES, SSE, LMM and LLM were obtained from Larodan Fine Chemicals AB (Malmö, Sweden), those of PSP, PPS, PSS and MMP were obtained from Unilever Research Laboratorium (Vlaardingen, The Netherlands). All samples were delivered as powders and then placed into glass capillaries. X-ray powder diffraction established all samples to be in the β-2 phase. The samples of LMM and PSS appeared to contain a small fraction of a β' polymorph, but annealing LMM at 318 K and PSS at 336 K was effective at removing this. PSP, as well as PEP, is β' stable (Lutton, 1972; Elisabettini *et al.*, 1998) and the β-2 polymorph is difficult to obtain. Methods used to obtain the β-2 phase of these particular samples could not be retrieved, but it is probably *via* crystallization from a solvent (Lutton & Hugenberg, 1960; Lutton, 1972).

HR-SPD data collection has been carried out at beamlines BM16 (PSP), BM01b (LLM, MMP, PEP, PPE, PSS, SES, SSE) and ID31 (LMM, PPS) at the ESRF (Grenoble, France). Non-ambient temperatures were controlled by an Oxford Instruments Cryostream (Abdingdon, England). At ID31 the cryostream was mounted horizontally to limit the temperature gradient along the capillary sample. At BM01b it was mounted with the gas-flow perpendicular to the capillary. The diameter (5 mm) of the cryogenic gas flow at BM01b limited the temperature-controlled length of the capillary to 4 mm. The continuous scans were binned with a step size of 0.005° 2θ.

Melting points have been determined by time-resolved and temperature-controlled laboratory X-ray powder diffraction (XRPD) using a PANalytical X'pertPro MPD diffractometer equipped with a sealed Cu X-ray tube, a primary elliptical mirror, an X'Celerator strip detector, 0.01 rad primary and secondary Soller slits, and a horizontally mounted Cryostream Compact (Oxford Instruments) to control the temperature of the capillary. An X-ray transparent cylindrical polymer foil guided the gas flow along the capillary to ensure a constant temperature along the irradiated part of the capillary. Samples were heated with 0.5 K min^{-1} and the changes in the diffraction pattern were monitored continuously in 1 min scans from 0.5–30° 2θ with a step size of 0.016° 2θ. In all experiments capillaries were spun continuously.

2.2. Indexing, model building, structure determination and refinement

The indexing of powder patterns of TAGs is complicated by dominant zone problems and severe peak overlap, as already explained in a previous publication (van Mechelen *et al.*, 2006*a*). The program *McMaille* (Le Bail, 2004) was used to index the diffraction patterns. The indexing was successful only after having limited the search space by applying restrictions to the allowed cell volume and axes lengths. The program *Chekcell* (Laugier & Bochu, 2001) was used to select and refine promising cells out of a list of proposed solutions produced by *McMaille*. The β-2 structures presented in this study were all indexed as being triclinic and the structures were solved in the space group $P\bar{1}$ with the program *FOX* (Favre-Nicolin & Černý, 2002) in a parallel tempering mode. A molecule can be decoded in *FOX* in two ways: as a molecule, comprising a list of atoms related to each other by bond distances and bond angles, or as a Z-matrix (Favre-Nicolin & Černý, 2002). The structure-solution process converges faster with a molecule description than with a Z-matrix description. However, manual intervention in structure-solution processes is much easier with a Z-matrix.[2] Since the number of resolved intensities in the diffraction pattern is small compared with the number of structural parameters, the generation of unrealistic molecular conformations by the structure solution program cannot be avoided completely. If a Z-matrix description of the molecule is used, an unacceptable molecular conformation can easily be rearranged into a more acceptable one by just modifying the torsion angles. The slower Z-matrix approach is the preferable choice for solving crystal structures of TAGs

[1] The carbon chain lengths are represented by the acronyms S: C18, P: C16, M: C14, L: C12 and E: C18:1 (*trans*-9).

[2] Recently a molecule manipulation utility has been added to *FOX* that facilitates manual intervention.

Table 1
Experimental and structural details of the structure refinement of β-2 structures of symmetric TAG molecules.

	β-2 SES	β-2 PEP	β-2 PSP
Chemical formula	$C_{57}H_{108}O_6$	$C_{53}H_{100}O_6$	$C_{53}H_{102}O_6$
M_r	889.47	833.38	835.39
Temperature (K)	250	250	295
a, b, c (Å)	5.425 (1), 11.95 (1), 44.64 (2)	5.417 (2), 12.13 (1), 41.54 (1)	5.439 (1), 12.18 (1), 41.60 (1)
α, β, γ (°)	92.01 (3), 88.76 (4), 100.18 (2)	88.31 (6), 92.09 (6), 99.95 (3)	88.73 (2), 93.10 (1), 99.97 (1)
V (Å^3)	2846.8 (2)	2685.2 (2)	2709.6 (1)
D_x (mg m^{-3})	1.04	1.03	1.02
T_m (K)	334	327	339.5
Specimen size (mm)	15 × 1.5 × 1.5	15 × 1.0 × 1.0	15 × 1.5 × 1.5
ESRF station	BM01b	BM01b	BM16
2θ range (°)	0.13–20.5	0.13–20.5	0.2–60.0
R factors and goodness-of-fit	R_p = 0.077, R_{wp} = 0.106, R_{exp} = 0.028, S = 3.99	R_p = 0.090, R_{wp} = 0.129, R_{exp} = 0.044, S = 3.03	R_p = 0.053, R_{wp} = 0.070, R_{exp} = 0.021, S = 3.64
λ (Å)	0.79984	0.79948	0.699716
No. of parameters	552	462	518
$(\Delta/\sigma)_{max}$	0.16	0.04	0.32

from powder diffraction data, at least in the early stages of the structure-solution process.

The TAGs discussed in this paper all crystallize in a chair-shaped conformation (Fig. 1). To distinguish between the various TAG conformations, the numerical identifier [$x - y$] is introduced, in which 'x' is the *sn* chain number (1–3) that is in the chair's back-leg position and 'y' is the *sn* chain number that forms the seat plus the front-leg position.

In accordance with published β-phase structures of tri-saturated TAGs (van Langevelde *et al.*, 1999, and references therein), molecular models in the *Z*-matrix description were built as [1–3] models. The starting conformation of the elaidoyl chain at the *trans* double bond was taken from the crystal structure of β-2 EEE (Culot *et al.*, 2000). This conformation does not differ much from the conformation of this chain in elaidic acid (Low *et al.*, 2005). Initially, the models were handled as rigid bodies but in the course of the structure-solution processes torsion-angle restraints at the central glycerol moiety and at the *trans* double bond were relaxed one by one. H atoms were included in the models only at the final stage.

Structure refinement was carried out with the program *GSAS* (Larson & Von Dreele, 1987) using a Chebyshev polynomial description of the background. The peak-shape function number four in *GSAS* allowed *hkl*-dependant line broadening and low-angle peak asymmetry to be studied. Soft restraints had to be applied to all bonding distances and angles including those of H atoms to stabilize the refinement. The weight of the restraints applied to H atoms was taken as half that of the weight applied to other atoms. Soft-planar restraints were applied to the saturated parts of the acyl chains. For the elaidoyl chain two planar restraints were defined, one for each carbon chain at both sides of the *trans* double bond. The restraint values for distances and angles were mean values taken from the Cambridge Structural Database (CSD; Allen, 2002). Displacement parameters have not been refined as tests with *cis*-mono-unsaturated TAGs (van Mechelen *et al.*, 2006*a*) and data of similar low resolution showed that this approach yields inconclusive results.

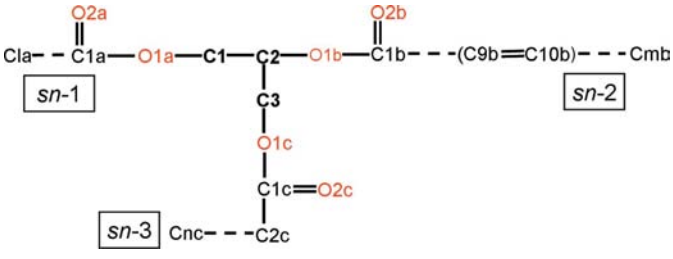

Figure 1
Chemical structure diagram of TAGs. The structural subscripts *l*, *n* and *m* (= 12, 14, 16 or 18) label the number of C atoms in the acyl chain. The example shows a [1–3] conformation with an elaidoyl chain in the *sn*-2 position (see the main text for the definition of [1–3]).

At the final stage of the refinements, the preferred orientation was refined using [001] as the preferred orientation direction. For most of the samples this did not improve the *R* values much, but for PSP it did (preferred orientation ratio 1.18). PSP has larger crystallites, as can be inferred from the smaller peak widths in the diffraction pattern. Investigation of the powder of PSP under a light microscope revealed it to consist of platelet-shaped crystals. A vibration tool that was used to fill the capillary may have oriented the rather thin, flat crystallites in the capillary causing the preferred orientation. The principal experimental and structural details are listed in Table 1 for the symmetrical TAGs and in Table 2 for the asymmetrical TAGs. The figures of the full traces of all patterns including the difference traces from the Rietveld refinements have been deposited.[3]

3. Results and discussion

3.1. Packing of the β-2 TAGs

The β-2 phase TAGs, the symmetric (SES, PEP and PSP) as well as the asymmetric ones (PPE, SSE, PPS, PSS, MMP, LLM

[3] Supplementary data for this paper are available from the IUCr electronic archives (Reference: DR5018). Services for accessing these data are described at the back of the journal.

Table 2
Experimental and structural details of the structure refinement of β-2 structures of asymmetric TAG molecules.

	β-2 SSE	β-2 PSS	β-2 PPS	β-2 PPE	β-2 MMP	β-2 LMM	β-2 LLM
Chemical formula	$C_{57}H_{108}O_6$	$C_{55}H_{106}O_6$	$C_{53}H_{102}O_6$	$C_{53}H_{100}O_6$	$C_{47}H_{90}O_6$	$C_{43}H_{82}O_6$	$C_{41}H_{78}O_6$
M_r	889.47	863.45	835.39	833.38	751.23	695.12	667.07
Temperature (K)	250	250	250	295	295	298	295
a, b, c (Å)	5.437 (1), 11.87 (1), 44.74 (2)	5.412 (2), 11.14 (3), 46.45 (4)	5.437 (1), 11.92 (2), 41.93 (2)	5.446 (1), 12.18 (2), 41.94 (2)	5.457 (2), 12.14 (2), 37.37 (2)	5.444 (1), 11.45 (1), 36.70 (2)	5.460 (2), 12.15 (1), 33.05 (1)
α, β, γ (°)	92.03 (3), 88.67 (4), 100.3 (2)	91.49 (6), 94.85 (6), 96.75 (3)	88.18 (4), 91.15 (4), 100.02 (3)	89.89 (6), 91.68 (6), 100.44 (2)	92.32 (5), 89.79 (5), 100.45 (3)	90.79 (2), 95.52 (3), 97.18 (2)	96.19 (3), 87.05 (3), 100.48 (2)
V (Å^3)	2837.5 (2)	2769.1 (3)	2675.3 (2)	2735.0 (2)	2432.6 (2)	2258.8 (2)	2141.5 (9)
D_x (mg m^{-3})	1.04	1.04	1.04	1.01	1.03	1.02	1.03
T_m (K)	333	338	335	320	327.5	320	316
Specimen size (mm)	4 × 1.5 × 1.5	4 × 1.0 × 1.0	2 × 1.5 × 1.5	2 × 1.5 × 1.5	15 × 1.5 × 1.5	1.5 × 2 × 2	15 × 1.5 × 1.5
ESRF Station	BM01b	BM01b	ID31	BM01b	BM01b	ID31	BM01b
2θ range (°)	0.14–20.5	0.14–31.5	0.5–60.0	0.53–40.5	0.52–53.3	1.3–50.0	0.53–35.0
R factors and goodness-of-fit	R_p = 0.072, R_{wp} = 0.096, R_{exp} = 0.048, S = 2.08	R_p = 0.079, R_{wp} = 0.11, R_{exp} = 0.020, S = 5.84	R_p = 0.083, R_{wp} = 0.11, R_{exp} = 0.030, S = 4.26	R_p = 0.048, R_{wp} = 0.068, R_{exp} = 0.020, S = 3.52	R_p = 0.056, R_{wp} = 0.076, R_{exp} = 0.021, S = 3.82	R_p = 0.056, R_{wp} = 0.076, R_{exp} = 0.050, S = 1.58	R_p = 0.048, R_{wp} = 0.064, R_{exp} = 0.011, S = 6.55
λ (Å)	0.79948	0.79948	1.25007	0.79936	0.85019	1.25007	0.800001
No. of parameters	556	546	517	520	467	429	408
$(\Delta/\sigma)_{max}$	0.11	0.13	0.49	0.5	0.34	1.12	0.21

and LMM), are packed in a chair-shaped [1–3] conformation (Fig. 1) so they adopt the same conformation as the trisaturated monoacid TAGs such as β-2 SSS and β-2 MMM (van Langevelde *et al.*, 2001*a*). The molecules are packed in symmetry-related pairs with the seats of the chairs facing each other, with an inversion point in-between the seats. The pairs of chairs form layers with a double chain-length thickness, referred to as 'two-packs'. The 'two-packs' face each other at the methyl end-plane.

Fig. 2 gives an overview of the complete diffraction patterns of the symmetric TAGs, while Figs. 3 and 4 show the fingerprint area (16–26° 2θ, for Cu $K\alpha_1$) of the symmetric and asymmetric TAGs, respectively (all 2θ values have been converted to the same Cu $K\alpha_1$-based scale). Below 15° 2θ the patterns are dominated by (00ℓ) reflections and the differences between the patterns are small. The line positions reflect the different average chain lengths of the molecules. The fingerprint area (Figs. 3 and 4) is dominated by three classes of reflections: (11ℓ), $(1\bar{2}\ell)$ and $(03\bar{\ell})$. These reflection groups correspond to chain layers, as can be visualized by rotating the crystal structure around the c axis (Fig. 5). In a view parallel to the chain direction, the orientation of the layers relative to the chain ordering becomes clear (Fig. 6). The pair of strong diffraction maxima at ~ 4.6 Å (19.5° 2θ, Cu $K\alpha_1$) that correspond to the (110) and (111) reflections is characteristic for triclinic β-2 structures of saturated TAGs and mono-unsaturated *trans* TAGs. The β-3 structures of mono-unsaturated *cis*-TAGs have only the (111) reflection at this position in the fingerprint area (van Mechelen *et al.*, 2006*a*,*b*, 2007). The (11ℓ)-zone reflections are related to the average plane defined

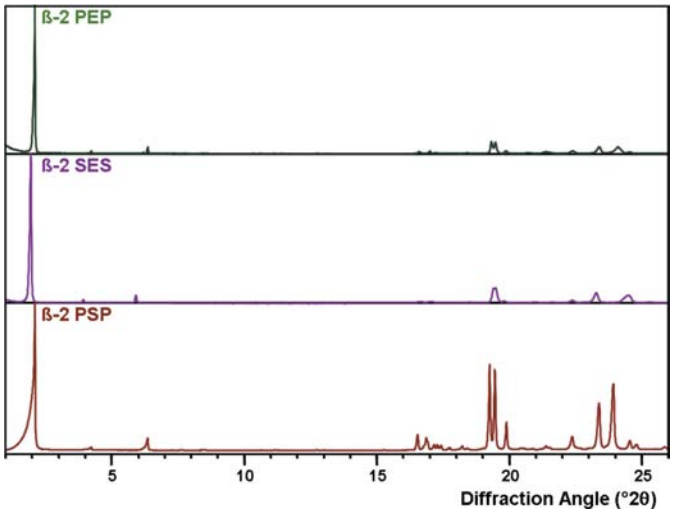

Figure 2
Overview of the β-2 patterns of symmetric TAG molecules with 2θ scale converted to Cu $K\alpha_1$ radiation.

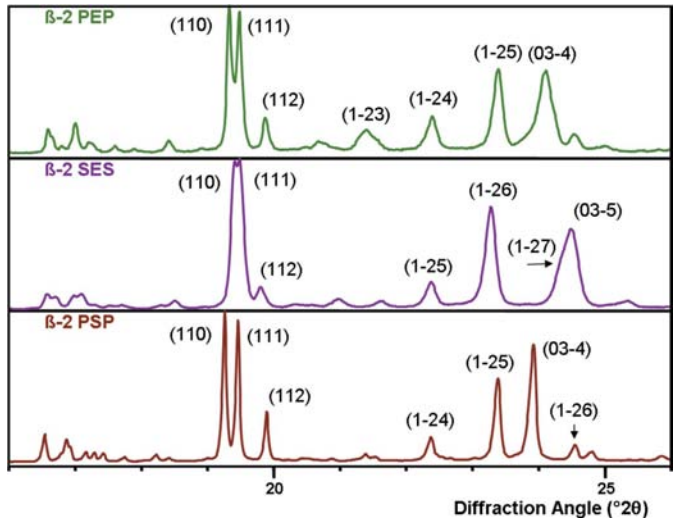

Figure 3
Fingerprint area of Fig. 2. The strongest peaks have been labelled with the Miller indices.

Table 3
Angles between step planes and acyl chains and alignment of acyl chains at the methyl end-plane for β-2 TAGs ordered by subgroup.

TAG	Subgroup	∠ step plane and *sn*-(1 + 2)	Aligned chains of methyl end-plane
PEP	$n\,n+2\,n$	48	⟨1–1⟩
PSP	$n\,n+2\,n$	49	⟨1–1⟩
PPE	$n\,n\,n+2$	80	⟨1–1⟩
PPS	$n\,n\,n+2$	78	⟨1–1⟩
MMP	$n\,n\,n+2$	80	⟨1–1⟩
LLM	$n\,n\,n+2$	80	⟨1–1⟩
PSS	$n\,n+2\,n+2$	82	⟨3–3⟩
LMM	$n\,n+2\,n+2$	75	⟨2–2⟩
SES	$n\,n\,n$	74	⟨2–2⟩
SSE	$n\,n\,n$	72	⟨2–2⟩

by the pair of molecules in the unit cell. This latter plane does not coincide with a Miller plane. The (111) reflection makes a small angle with this average plane (Fig. 5*c*). The (110) reflection also makes a small angle with the average molecular plane, but intersects it between the seats of the molecule pair. Although the zero ℓ index may suggest otherwise, the d spacing of the (110) reflection depends on the chain length (Fig. 7) while, remarkably, the d-value of the (111) reflection shows no such dependence on the chain length. This situation is similar to that found in *cis*-mono-unsaturated β-3 structures. LMM and PSS are outliers in Fig. 7 owing to a difference in the packing, as discussed in §3.3.

3.2. The methyl end-plane

The 'two-packs' that face each other at the methyl end-plane are shifted over $\frac{1}{4}$ along the a axis relative to each other. This shift, shown in Fig. 5(*c*), is typical for all β-2 TAGs discussed in this work and is also found in the ($n\,n\,n$) (n = even) group of TAGs. In contrast, in the ($n\,n\,n$) (n = odd) type TAGs almost no shift is present (van Langevelde *et al.*, 2001*b*; Helmholdt *et al.*, 2002).

When viewed parallel to the a axis, the chair-leg acyl chains of TAGs at opposite sides of the methyl end-plane are aligned. Alignment of chair-leg chains *sn-i* and *sn-j* ($i, j = 1, 2, 3$) will be denoted as ⟨*i*–*j*⟩. The different acyl chain lengths of the β-2 TAGs lead to differences in methyl end-plane shapes and acyl-chain alignments. For example, at the methyl end-plane some differences between SES and PEP can be discerned (Fig. 8). SES has an ⟨2–2⟩ alignment of the elaidoyl chains that form the back of the chair (Table 3). The methyl end-groups of the *sn*-1, *sn*-2 and *sn*-3 chains in β-2 SES, in this order, lie close to a common plane, from now on referred to as the step plane. Between *sn*-3 and *sn*-1 there is a small step. (Fig. 8*b*). The step plane in the methyl end-plane of SES is not far from being

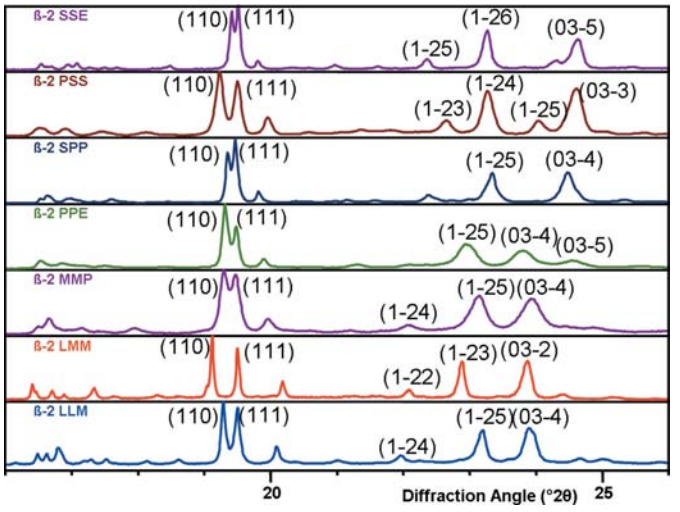

Figure 4
Fingerprint area of asymmetric β-2 TAG structures rescaled to Cu $K\alpha_1$ radiation and Miller indices for the strong reflections.

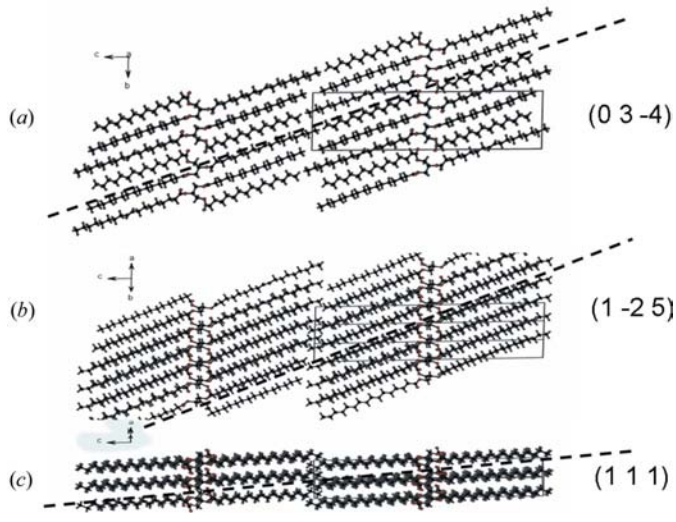

Figure 5
Packing of PEP. Rotation of the structure around the c axis shows the chain layers that correspond to the three dominant zones of the fingerprint area: (*a*) (03$\bar{4}$), (*b*) (1$\bar{2}$5) and (*c*) (111).

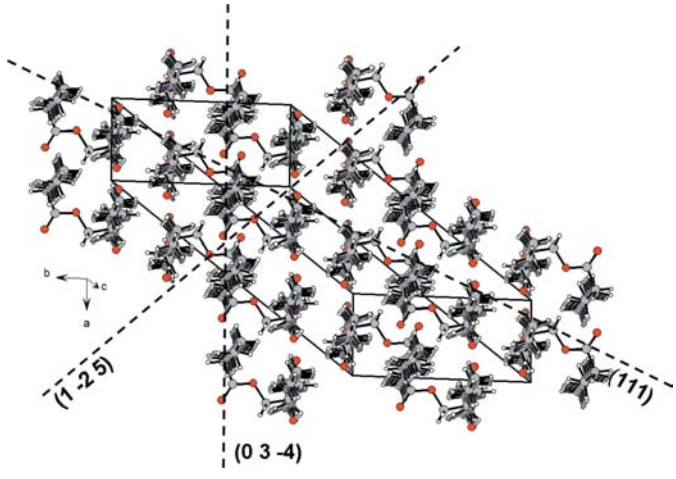

Figure 6
PSP: a view with the chains perpendicular to the paper showing the orientation of the dominant planes in the fingerprint area of the diffraction pattern.

perpendicular to the chains it is formed by (74°, Table 3), making the step size quite small. The β-2 PEP has the same packing of the seats relative to the inversion centre, but different saturated chain lengths. Without any conformational changes, the shorter legs of the chair would have resulted in large empty spaces at the methyl end-plane arrangement of SES. However, the step plane in PEP has a different sequence (*sn*-3, *sn*-1, *sn*-2) with a step in between *sn*-2 and *sn*-3 (Fig. 8*a*). To make the opposing steps and step planes coincide, the 'two-packs' in PEP have become tilted, resulting in a ⟨1–1⟩ alignment.

Lutton postulated that for mixed-chain-length TAGs, with n and/or $n + 2$ C atoms (n even) and similar molecular conformations, the shape of the methyl end-plane should not change because the end-plane is stepped and only the position of the step changes with a difference in chain length (Lutton, 1971, 1972). An ⟨*n*–*n*⟩ alignment of chains marks the centres of the three possible step-plane positions. In Table 3 the aligned chains have been tabulated for the β-2 structures of this publication, arranged according to the TAG subgroup. The alignment agrees well with the postulations of Lutton, except for LMM (see §3.3).

The packing at the methyl end-plane and the position of the step plane have an important influence on the melting point (T_m) of the TAGs. The equal chain length β-2 structures known to date all have a stepped surface. When for a homologous series of TAGs this surface is the same for all members of the series, the relation between the melting point and the chain length of the acyl chains is expected to be a continuous function, as pointed out by Lutton & Fehl (1969). Fig. 9 shows the relation between the melting point T_m and the length of the c axis for the β-2 crystal structures solved by us and those published by others for (*n n n*) (*n* = even)-type TAGs. The number of items per subgroup is too small to calculate trend lines, but by interconnecting the datapoints of adjacent members of a subgroup by straight lines trends within a subgroup and differences between subgroups become visible. Each subgroup has its own characteristic methyl end-plane packing and a related subgroup-specific melting-point trend.

For the subgroups of saturated TAGs the melting points decrease in the order T_m (*n n n*) > T_m (*n n* + 2 *n*) > T_m (*n n* + 2) > T_m (*n* + 2 *n* + 2) (Fig. 9). The melting points of the E-containing analogues are more than 10 K below the saturated ones. The unit-cell dimensions of all the E-containing samples agree well with trends of the β-2 series (Fig. 10, open markers).

In SES and PEP the E chain at the *sn*-2 position forming the back of the chair just replaces the saturated *sn*-2 S chain in PSP. The *trans* double bond seems not to distort the flatness of

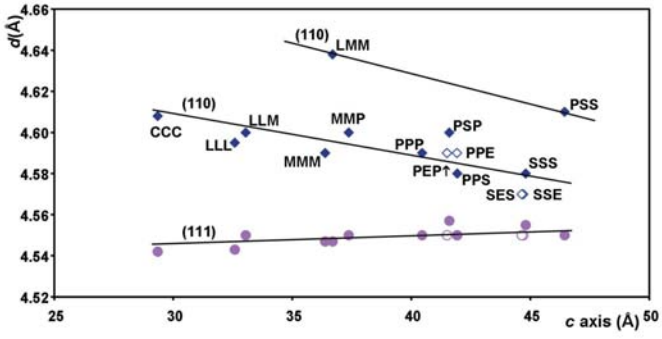

Figure 7
d values of (110) and (111) reflections as a function of the *c* axis. The straight lines are trend indicators.

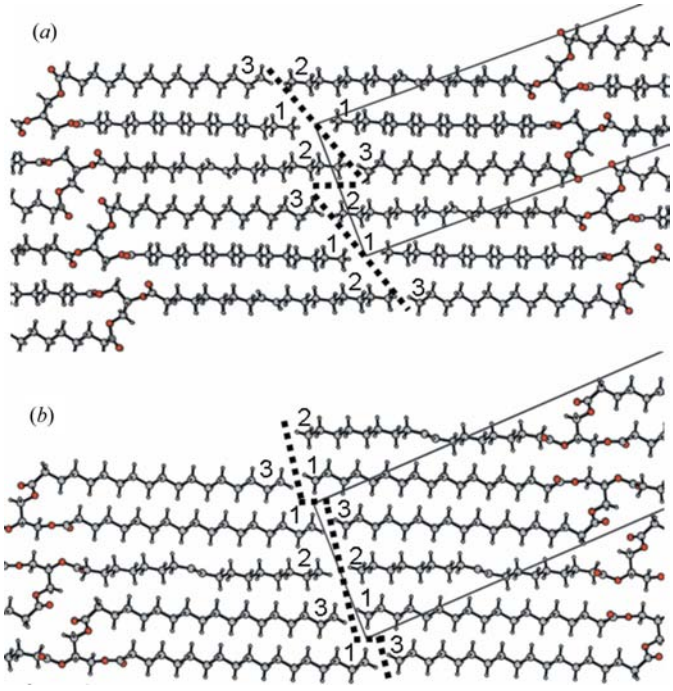

Figure 8
Methyl end-plane of (*a*) PEP and (*b*) SES with *sn* numbers of chains; view parallel to the *a* axis. Step planes and steps at the methyl end-plane are marked by a dotted line.

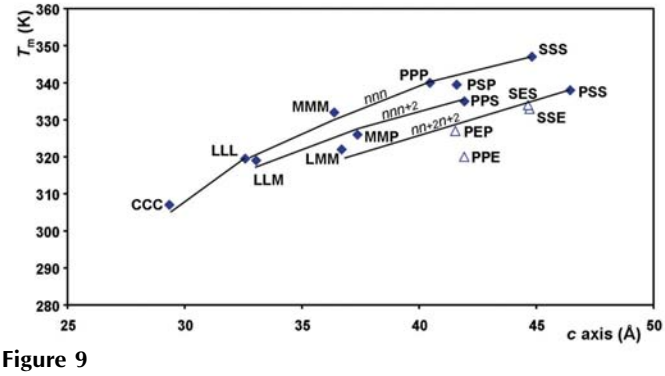

Figure 9
Relation between β-2 melting point and length of the *c* axis. Datapoints of the same subgroup of TAGs have been connected to visualize the trend. The *c* axes of the (*n n n*) class of TAGs have been taken from the literature (van Langevelde *et al.*, 1999) and subjected to the transformation matrix (001\100\$\bar{2}\bar{1}$2). Original cell dimensions (Å, °) *a*/*b*/*c*/α/β/γ: SSS 12.005/51.902/5.445/73.75/100.26/117.69; PPP 11.95/46.84/5.45/73.8/100.2/118.1; MMM 12.063/41.714/5.4588/73.388/100.41/118.27; CCC 12.18/31.56/5.49/73.4/100.7/119.2; LLL 12.08/36.61/5.47/73.4/100.5/118.7.

the chain enough to modify the molecular conformation in the β-2 packing.

In β-2 PEP as well as β-2 PSP, the angle between the step plane and the chains is considerably smaller than in β-2 SES and the asymmetric TAGs (48, 49°; Table 3), making the step size so large that an interdigitated 'two-pack' pattern at the interface results (Fig. 8*a*). This energetically unfavourable methyl end-plane may explain why the melting points of β-2 PEP (327 K) and β-2 PSP (339.5 K) are lower than the melting points of β'_1-2 PEP (329 K) and β'_1-2 PSP (343 K), respectively (see paper IV in this series; van Mechelen *et al.*, 2008). Interestingly, when crystallizing from a melt, the opposite occurs, with melting points of β phase(s) that are higher than those of the β' phase(s). The methyl end-plane configuration in β-2 PEP and β-2 PSP is of the same type as postulated for mixed palmitic stearic TAGs (Lutton, 1971).

In the [1–3] structural model found for SSE and PPE, the E chain is packed parallel to an S chain in the seat and front leg of the chair. This is the usual β-2 conformation. The alternative [1–2] model in which the *sn*-3 elaidoyl chain is at the back of the chair, instead of in the seat and front-leg position, has also been investigated for PPE as well as SSE. However, in spite of extensive testing, a conformation was not found for either PPE or SSE that fitted the diffraction data better than the model with *sn*-3 in the seat plus front-leg position for both.

Thus, at the given resolution of the data it is concluded that an elaidoyl chain can easily replace a stearoyl chain without major conformational changes. The parts of the E chain on both sides of the double bond (Fig. 1) are aligned within the resolution of the diffraction data and also in this respect no difference with saturated (P, S) chains can be observed that may explain the lower melting points of the E-containing TAGs.

3.3. The packing of LMM and PSS

LMM and PSS are members of the class of TAGs ($n\ n+2\ n+2$), of which the β phase melting points are higher than or equal to those of the β' phase (Hagemann, 1988; Lutton, 1950), suggesting that the β phase is the most stable. Interestingly, Sato *et al.* (2001) reported PPM (in our notation: MPP), also a member of this class of TAGs, to be β' stable and even solved a β' phase crystal structure from single-crystal data. Kodali *et al.* (1990) did not succeed in obtaining the β phase either. Apparently, the β polymorph of this class of TAGs is difficult to obtain. From the annealing experiments carried out with LMM and PSS, both initially consisting of a β'/β mixture, it was obvious that the β' polymorph melted while the β polymorph did not, thus showing unambiguously that the β phase is the most stable of this type of TAG.

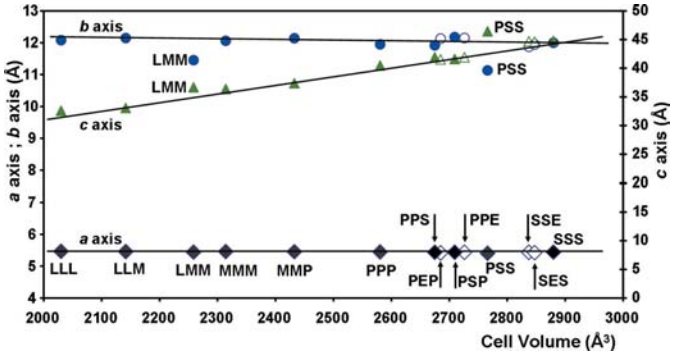

Figure 10
Unit-cell dimensions as a function of the cell volume.

As stated, PSS and LMM are outliers in Fig. 7 as their (110) *d* spacing is approximately 0.04 Å above the trend line through the (110) *d* spacings of the other TAGs. This indicates that their molecular packing differs from that of the other β-2 TAGs. An analysis points out that this is indeed the case. Both PSS and LMM have a shorter *b* axis, while PSS also has a longer *c* axis than indicated by the trend lines (Fig. 10). When in Fig. 9 the *c* axis scale is replaced by a cell-volume scale the two trend lines for saturated asymmetric TAGs merge into one. The influence of the difference in packing on T_m is limited, thus allowing for a common trend line of T_m *versus* the cell volume for the two asymmetric sub-groups, within the accuracy of the available data. The T_m trend line for even-numbered saturated ($n\ n\ n+2$) plus ($n\ n+2\ n+2$) TAGs is 7 K below that of ($n\ n\ n$) TAGs and that of *trans*-mono-unsaturated TAGs approximately 15 K. The single datapoint obtained for the ($n\ n+2\ n$) subgroup (PSP) does not allow for a trend line. The PSS and LMM molecules form seat-facing symmetry-related pairs and have the same [1–3] conformation as the other β-2 TAGs. The pairs, however, are shifted relative to each other along and parallel to the back of the seat. According to Lutton (1971), members of this subgroup are expected to have a ⟨3–3⟩ alignment at the methyl end-plane and PSS indeed shows this alignment (Table 3). LMM, however, has a ⟨2–2⟩ alignment and this is not in line with this postulation. When the steps at the methyl end-plane are located in between two chains of a seat-facing symmetry-related pair, the internal rigid structure of the pairs does not allow a conformational change that would remove the step and would create an energetically favourable flat methyl end-plane. Hence, the opposing steps at both sides of the methyl end-plane are moved to make them fit like a jigsaw puzzle. In PSS the step plane at the methyl end-plane is formed by a single seat-facing pair with *sn*-3 as the middle chain, resulting in the expected ⟨3–3⟩ alignment. The seat-facing pairs are shifted relative to each other, compared with those of other TAG subgroups, and this shift resulted in a flat methyl end-plane. In projection on the *ac* plane the seats of back-facing molecules are aligned and not shifted, unlike the other β-2 structures. The inclination of the chains with the long axis does not differ much between LMM and PSS (Table 3), and also the orientation of the molecules in the respective cells hardly changes. If in PSS the chains and the *c* axis would be shortened to the length of LMM, while keeping a constant inclination with the *c* axis, the chain alignment at the methyl end-plane would change from ⟨3–3⟩ into ⟨2–2⟩. This explains the unexpected ⟨2–2⟩ alignment of LMM. The stepless terrace structure of the ($n\ n+2\ n+2$)-type TAGs has been proposed by de

Jong & van Soest (1978) as one of the two packing possibilities according to their β-2 packing theory.

3.4. The problem of local minima

The determination of the crystal structures of TAGs from HR-SPD data is complicated because of the peak overlap and dominant zone problems. As explained in a previous publication (van Mechelen *et al.*, 2006*a*), in view of the (non-atomic) resolution of the data one should be aware of local minima, implying that the molecular conformations and types of packing found by *FOX* do not necessarily correspond to those of the absolute minimum. Problems with local minimum conformations have also been encountered for the β-2 structures discussed here. The ordering of the long acyl chains creates a diffraction pattern that is dominated by a few zones. Positional information of the atoms in the glycerol moiety (comprising the 'seat' of the chair) is obscured by these rather broad reflections. The seat is the interconnection between the columns of electron density formed by the acyl chains and since its orientation cannot be established unequivocally (by *FOX*) at the stage of structure solution because of the limited resolution of the data, options for alternative models should be kept open. As an example, in Fig. 11 a structural model of LMM with an improper seat orientation is shown. The seat of the chair is oriented more or less parallel to the zigzag plain of the acyl chains. In view of the β-2 type of packing, this conformation is unlikely to be correct as it deviates from the perpendicular orientation found in β-2-type single-crystal structures, *e.g.* EEE (Culot *et al.*, 2000) and PPP (van Langevelde *et al.*, 1999). Nevertheless, this model refined smoothly to a quite acceptable final $R_{\rm p}$ of 0.075. Attempts to rotate the acyl chains around the length axis to explore a possible rotational freedom within the envelope of the overlapping reflections of the HR-SPD pattern, as found in the β-3 TAGs, unambiguously led to higher R values. To escape this local minimum the molecule had to be rotated 'manually' in *FOX* around the length axis of the back, including the back-leg chains of the chair as indicated in Fig. 11. This modified model refined to a significantly lower $R_{\rm p}$ (0.056) and has a molecular conformation that agrees well with the published single-crystal β-2 structures referred to above (Fig. 11).

The absence of a bend in the back of the seat creates another local minimum problem. The TAGs are ordered in pairs of chairs with the seats facing each other and an inversion centre in between the seats. When such a pair of chairs is rotated 180° around an axis through the inversion centre and perpendicular to the backs of the seats, the columns of electron density of the acyl chains are hardly affected. The 'major' changes are found at the position of the seats and at the methyl end-plane (note: the rotation axis is not parallel to the methyl end-plane). An indication for the correctness of the packing can be found by inspection of the methyl end-plane. For example, for PPE a $\langle 1\text{–}1\rangle$ alignment at the methyl end-plane has been predicted (Lutton, 1971). The PPE model found initially with *FOX* had an $\langle 2\text{–}2\rangle$ alignment, but after rotating the molecule manually in *FOX*, as described above, the $\langle 1\text{–}1\rangle$ alignment was obtained and eventually the final R value of this model became lower than that of the initial $\langle 2\text{–}2\rangle$ alignment model.

4. Conclusions

A set of 10 β-2-phase crystal structures of TAGs, with mixed-acyl chain length ($\Delta n \leq 2$), an even number of C atoms and in four cases an elaidoyl chain instead of a saturated one has been solved from HR-SPD data. The strong reflections in the fingerprint area of the diffraction patterns are explained as dominant zones related to the layered packing of acyl chains. The molecular conformation is equal to the β-2 molecular conformation of equal chain-length trisaturated TAGs. Replacement of a saturated S chain by the *trans*-mono-unsaturated E-chain turned out to have no significant influence on the packing of the β-2 phase, in spite of a decrease of the melting point of more than 10 K. Molecular packings postulated by Lutton are confirmed by the crystal structures, except for the $(n\ n+2\ n+2)$ subgroup. The shift of pairs of chairs along the back was postulated, but the different packing of LMM is a surprise. The aberrant interdigitated 'two-pack' methyl end-planes found for β-2 PSP and β-2 PEP, normally β' stable materials, may explain the unusual stability of these TAGs.

Structure solution and refinement of TAGs from HR-SPD data are by no means routine. Due to the limited resolution the structure solution process may become locked in local minima and a continuous critical assessment of the solved structures is required. In this respect, solving a homologous series of structures may help to recognize local minima. In spite of the limited resolution of data, crystal structure solution of these TAGs using HR-SPD data has turned out to be feasible.

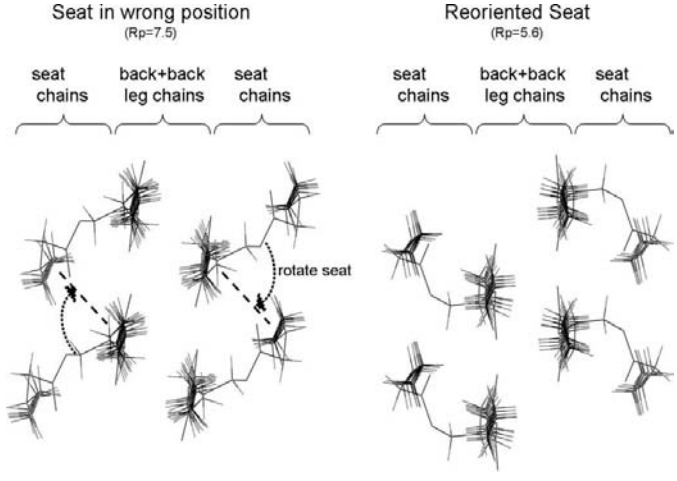

Figure 11
Rotation of the seat chain of LMM around the back plus back-leg chains to escape from a local minimum in the structure solution process.

The authors thank Unilever Research Vlaardingen for supplying the pure triglycerides. The authors acknowledge the ESRF (Grenoble, France) for providing the facilities to perform the synchrotron diffraction experiments and they thank W. van Beek (Swiss–Norwegian CRG beamline BM01b), O. Masson (former beamline BM16) and I. Margiolaki (beamline ID31) for their valuable help during the experimental sessions. The authors also thank E. Dova, K. Goubitz, R. B. Helmholdt, E. Sonneveld and M. M. Pop for their help in data collection during various experimental sessions. The investigations have been supported by the Netherlands Foundation for Chemical Research (NWO/CW) with financial aid from the Netherlands Technology Foundation (STW) (project 790.35.405). The members of the User Committee of this project are thanked for stimulating discussions and continuous interest.

References

Allen, F. H. (2002). *Acta Cryst.* B**58**, 380–388.
Björkbom, A., Ramstedt, B. & Slotte, J. P. (2007). *Biochim. Biophys. Acta (BBA) Biomembranes*, **1768**, 1839–1847.
Culot, C., Norberg, B., Evrard, G. & Durant, F. (2000). *Acta Cryst.* B**56**, 317–321.
Elisabettini, P., Lognay, G., Desmedt, A., Culot, C., Istasse, N., Deffense, E. & Durant, F. (1998). *J. Am. Oil Chem. Soc.* **75**, 285–291.
Favre-Nicolin, V. & Černý, R. (2002). *J. Appl. Cryst.* **35**, 734–743.
Gibon, V., Blanpain, P., Norberg, B. & Durant, F. (1984). *Bull. Soc. Chim. Belg.* **93**, 27–34.
Hagemann, J. W. (1988). *Crystallization and Polymorphism of Fats and Fatty Acids*, edited by N. Garti & K. Sato, pp. 9–95. New York: Marcel Dekker, Inc.
Helmholdt, R. B., Peschar, R. & Schenk, H. (2002). *Acta Cryst.* B**58**, 134–139.
Jensen, L. H. & Mabis, A. J. (1966). *Acta Cryst.* **21**, 770–781.
Jong, S. de & van Soest, T. C. (1978). *Acta Cryst.* B**34**, 1570–1583.
Kodali, D. R., Atkinson, D. & Small, D. M. (1990). *J. Lipid Res.* **31**, 1853–1864.
Langevelde, A. van, van Malssen, K., Hollander, F., Peschar, R. & Schenk, H. (1999). *Acta Cryst.* B**55**, 114–122.
Langevelde, A. van, Peschar, R. & Schenk, H. (2001*a*). *Acta Cryst.* B**57**, 372–377.
Langevelde, A. van, Peschar, R. & Schenk, H. (2001*b*). *Chem. Mater.* **13**, 1089–1094.
Larson, A. C. & Von Dreele, R. (1987). *GSAS*, Report No. LAUR-86-748. Los Alamos National Laboratory, New Mexico, USA.
Larsson, K. (1965). *Archiv Kemi*, **23**, 1–15.
Laugier, J. & Bochu, B. (2001). *Chekcell*; http://www.inpg.Fr/LMPG.
Le Bail, A. (2004). *Powder Diffr.* **19**, 249–254.
Low, J. N., Scrimgeour, C. & Horton, P. (2005). *Acta Cryst.* E**61**, o3730–o3732.
Lutton, E. S. (1950). *J. Am. Oil Chem. Soc.* **27**, 276–281.
Lutton, E. S. (1971). *J. Am. Oil Chem. Soc.* **48**, 245–247.
Lutton, E. S. (1972). *J. Am. Oil Chem. Soc.* **49**, 1–9.
Lutton, E. S. & Fehl, A. J. (1969). *Lipids*, **5**, 90–99.
Lutton, E. S. & Hugenberg, F. R. (1960). *J. Chem. Eng. Data*, **5**, 489–490.
Mechelen, J. B. van, Peschar, R. & Schenk, H. (2006*a*). *Acta Cryst.* B**62**, 1121–1130.
Mechelen, J. B. van, Peschar, R. & Schenk, H. (2006*b*). *Acta Cryst.* B**62**, 1131–1138.
Mechelen, J. B. van, Peschar, R. & Schenk, H. (2007). *Acta Cryst.* B**63**, 161.
Mechelen, J. B. van, Peschar, R. & Schenk, H. (2008). *Acta Cryst.* B**64**, 249–259.
Sato, K., Goto, M., Yano, J., Honda, K., Kodali, D. R. & Small, D. M. (2001). *J. Lipid Res.* **42**, 338–345.